Velocity Variation of Opak Fault GNSS Observation Station 2006 Yogyakarta Post-Earthquake

Velocity Variation of Opak Fault GNSS Observation Station 2006 Yogyakarta Post-Earthquake

Nurrohmat Widjajanti[1], Septi Praja Abdiana[2], Parseno[1], Cecep Pratama[1]

[1]Lecturer, Department of Geodetic Engineering Universitas Gadjah Mada Yogyakarta, Indonesia
[2]Student, Department of Geodetic Engineering Universitas Gadjah Mada Yogyakarta, Indonesia

nwidjajanti@ugm.ac.id, septi.praja.abdiana@mail.ugm.ac.id, parseno@ugm.ac.id, cecep.pratama@ugm.ac.id

Abstract. The postseismic effects of the 2006 Yogyakarta earthquake was caused by the Opak Fault activity as the possible source still continues. Secular velocity analysis who referred to the velocity which is free from the other deformations than interseismic deformation needs to be done to represent local deformation of the fault. This study was conducted to determine the significance of the difference between the secular velocity without and with postseismic corrections. The secular velocity is determined by the linear least square method. Furthermore, the velocity is calculated its postseismic correction with logarithmic method. This research data includes CORS BIG and Opak Fault station observation data from 2013 to 2018 which is processed using GAMIT/GLRED. Furthermore, the time series data for each station is plotted and analysed, then it is visualized its velocity. The result of this study shows the value of secular velocity each station ranges from 21.676 to 30.997 mm/year and -14.116 to. 2.573 mm/year in the East (E) and North (N) components respectively, and the resultant value of the horizontal velocities range from 22.507 to 32.711 mm/year. The secular velocity resulted with postseismic correction range from 20.735 to 29.864 mm/year and -22.255 to -6.439 mm/year in E and N components, and the resultant value of the horizontal velocities range from 36.963 to 23.281 mm/year. The velocities difference value in the E and N components range from -4.876 to 1.915 mm/year and -1.543 to 14.175 mm/year, and the horizontal velocities values range from -11.035 to 1.260 mm/year. The statistical significance of the two-parameter differences of the whole station, it is concluded that there was no significant velocities difference between the secular velocity values without and with postseismic corrections.

1. Introduction

Java Island has a geological structure that is dominated by strike slip and normal faults. One of the active faults in Java is the Opak Fault. The fault is a sinistral shear fault that extends southwest-northeastward turning eastward and joins the inactive Batur Agung upward fault system (Pusat Gempa Nasional, 2017). The existence of the fault has actually been discovered since 1980 by geologists in the Gunung Kidul area. This fault was active again in 2006 and is still active until now, marked by the occurrence of shocks in the fault area.

One of the earthquake disasters that had occurred was the earthquake on May 27, 2006 in the Special Region of Yogyakarta (DIY) with a magnitude of 6.3 Mw which resulted in 6234 people died (Pusat

Gempa Nasional, 2017). USGS recorded that the earthquake occurred at 05:53:58 WIB with the epicenter position of 7.97ºS and 110.44ºE, with a depth of 10 km. This earthquake is thought to have occurred due to tectonic activity from the fault or often called the Opak Fault. The fault extends from Parangtritis Beach to Prambanan.

Annual observations on the fault have been carried out by a research team from the Geodetic Engineering Department, Faculty of Engineering, Universitas Gadjah Mada with geometric aspect monitoring. GNSS observations have been carried out from 2013 to 2018. Twenty-three stations were installed in the fault area. The monitoring stations scattered around the fault are used for represents movement geometric (Widjajanti, et al., 2018, Widjajanti, et al., 2020). The measurement to produce information about the magnitude and surface shear velocity of each GNSS observation station. Thus, each year the changes in the position of GNSS observations can be used to analyze changes from year to year.

Earthquakes have a cycle that keeps repeating themself. Earthquakes that occur in an area can occur again in the future within a certain period of time. The phases of the earthquake recurrence can be divided into phases interseismic, coseismic, and postseismic (Pusat Gempa Nasional, 2017). Over time the earthquake phase can return to the initial phase, namely the interseismic phase. In this case, interseismic phase is the phase when the linear deformation is a result of plate movement, which is often referred to as secular deformation. So far, the deformation analysis of the Opak Fault only explains the velocity of ordinary deformations without considering the effects of other deformations. This causes the magnitude of the original or secular deformation that occurred in the fault is not known with certainty. In order to obtain a velocity value that is free from the effects of other deformations, it is necessary to calculate it secular velocity. Therefore, the estimation of the secular movements is needed causes of the emergence of earthquakes are not fully understood, especially those related to the secular GNSS movement (Heliani, et al., 2019).

Based on research (Abidin, et al., 2009) effects of the 2006 Yogyakarta post-earthquake continued for several years afterwards. The potential for earthquakes that occur in Yogyakarta causes the need for disaster mitigation efforts. One form of disaster mitigation for people in earthquake zones is to model the potential for earthquakes by monitoring geodynamic activity with GNSS observations. Through GNSS observations of deformation movements that occur after the earthquake (postseismic) can be known. The postseismic deformation definition is deformation due to the phase after the main earthquake occurs where the remaining energy is released aseismically (not earthquake activity).

Similar studies that have been conducted have only focused on ordinary deformation analysis such as the calculation of ordinary displacement, strain, and velocity, but in fact, there are still important deformation parameters besides strain and displacement, namely secular velocity. Secular deformation is the linear deformation due to plate tectonic processes such as plate movement, deformation interseismic, and block rotation. Secular deformations tend to be spatially broadly distributed and can be modeled with high precision within a frame of reference (Stanaway, et al., 2012).

A secular velocity analysis is necessary to represent the local deformation of the fault. The secular velocity referred to is the velocity that is free from deformations other than interseismic deformation. Secular velocity is a phase interseismic that oftentimes mixed with postseismic due to the vulnerability of the fast time. Secular velocity is also affected by seasonal variation and local movements. However, in the case of the Opak Fault, it can be eliminated postseismic because based on research (Abidin, et al., 2009) influence postseismic the 2006 Yogyakarta earthquake continued for several years after the earthquake. Therefore, this study examines secular velocities that show the true geodynamic pattern without any interference from effects postseismic. After that, the data processing uses scientific software to determine the comparison of the secular velocity movement without correction with the secular velocity of the correction postseismic, then it can be seen the significance of the difference between the secular velocity without and with postseismic corrections.

2. Data and Methods

2.1. Data and Location

This research was conducted in the Opak Fault area in the Yogyakarta Special Region. The data include:

1. RINEX data of the Opak Fault in the 2013 to 2018 of GNSS data campaign observation by the research team of the Geodetic Engineering Department, Faculty of Engineering, Universitas Gadjah Mada.
2. Continuous observation data of CORS Yogyakarta station includes Bantul station (CBTL) and Citengan BMKG Yogyakarta station (JOGS) which are downloaded via https://srgi.big.go.id.
3. RINEX data of CORS Yogyakarta station (JOG2) and monitoring data for IGS stations are downloaded via ftp://cddis.gsfc.nasa.gov or ftp://garner.ucsd.edu. The IGS station consists of COCO, CUSV, DARW, DGAR, GUAM, NTUS, KARR, PIMO, XMIS, IISC, and BAKO. The data is used for connection point of the monitoring station Opak Fault.
4. Broadcast ephemeris data in * .yyn format are downloaded via ftp://cddis.gsfc.nasa.gov. The data contains satellite navigation data.
5. Presice ephemeris data in *.sp3 format are downloaded via ftp://cddis.gsfc.nasa.gov. This data contains final orbit data for determining the satellite orbit.
6. Weather modelling correction data is in the format vmf1grid.YYYY, tide data is in the otlFES2004.grid format, and atmospheric modelling data in atmdisp_cm.YYYY format. The data are downloaded via ftp://everest.mit.edu/pub/GRIDS/.
7. Earthquake data from 2013 to 2018 that occurred in Yogyakarta with magnitudes ranging from 4.1 Mb to 4.4 Mb based on USGS data are downloaded via https://earthquake.usgs.gov.

2.2. Methodology

This research used data displacement of CORS CBTL and JOGS BIG stations. The processing of the CORS JOG2 station and the campaign data for the Opak Fault observation stations are done using GAMIT/GLRED. The main file is the observation data file in the form of RINEX data at each observation station. The RINEX data have been quality checked with TEQC.

GAMIT processing is carried out automatic batch processing, namely processing GAMIT automatically in one command, so that it can make processing easier. Automatic batch processing processes the data loose-constraint according to the files that have been prepared previously. GAMIT processing results are evaluated by looking at the values of postfit nrms and fract contained in q-files doy each on all projects. GAMIT processing is accepted if the value postfit nrms < 0.25 and value fract < 10. The value fract > 10 indicates a blunder error, the a priori coordinate value is not correct, or the constraint given is not correct, while the postfit nrms value> 0.25 indicates an error during modeling, there are still errors that have not been evenly distributed, or the existence of cycle slips that have not been distributed. well resolved (Herring, et al., 2010). If both conditions are met, the h-files solution can be used in further processing with GLOBK.

The processing with GLOBK use the GLRED module. The results of previous GAMIT processing are used as input for processing on GLRED. Evaluation of this processing can be seen from the wrms value contained in the time series plot and the coordinate standard deviation value. The tolerance limit of the wrms value is 10. If the wrms value is more than 10 then the GAMIT/GLOBK processing needs to be further evaluated.

The result of GLRED processing is in the form of daily solution stochastic (time series). GAMIT/GLRED produces the coordinates of observation stations in a 3D cartesian (X, Y, and Z) and a topocentric coordinate systems. In this study, topocentric coordinates were used for analysis. The results of the time series are then processed to obtain velocity values.

The evaluation of goodness of fit use the value of the Root Mean Square error (RMS error). The RMS error value is used to evaluate the suitability of the model used. The RMS error value is close to 0, indicating that the model has a smaller random error component and has a better suitability for prediction.

The velocity and standard deviation of the Opak Fault observation station are calculated using linear least square method, which uses a linear function approach with topocentric coordinate data (Maiyudi, et al., 2017). The characteristics of the linear least square method are modeled by equation (1).

$$y = ax + c \tag{1}$$

In this case,
y : data at the time of observation
a : secular velocity vector
x : time of observation (year doy/365)
c : displacement value in the first moment (offset)

The velocity value is obtained automatically in the linear least square method script. The data are in the topocentric coordinate system, with input in the form of coordinate displacement data and the time of observation. Then the secular velocity parameter is searched by the least square parameter method according to equation (2).

$$X = (A^T PA)^{-1}.(A^T PF) \tag{2}$$

A is a design matrix that contains the linearization of the equation to the parameters. F is the observation matrix, and the X matrix is the parameter (a and c), where a is the magnitude of the displacement, while P is the weight matrix.

In equation (2), the X matrix contains the parameters, namely a and c, where a is the secular velocity and c is the coseismic offset. Matrix A contains the first derivative of equation (1) to the parameter, while the matrix P is the weight matrix, and the matrix F is the observation matrix. For one doy, the X matrix order is 2x1, so if for one station, the X matrix order obtained is 2x1 multiplied by the number of doy for each station.

The determination of the velocity value of the postseismic correction use the logarithmic method, first determining the velocity value on the continuous CORS Yogyakarta data. The stage determines the velocity value, the estimated decay time log (tlog) for postseismic parameters such as the amplitude (b) value is also searched with these continuous data. Furthermore, the estimation results of rational tlog and b from these continuous data are made fixed to estimate the results of campaign observation data.

In further analysis, the GNSS time series displacement modeling is carried out with a logarithmic function. Logarithmic function is a function with the independent variable in the form of logarithms. This function can be used to determine postseismic parameters after the earthquake. Postseismic deformation characteristics can be modeled with a logarithmic function as in equation (3) (Feng, et al., 2015; Marone, et al., 1991):

$$u(t) = a + b\ log\left(1 + \frac{t-tq}{t\ log}\right) + c \tag{3}$$

In this case,
$u(t)$: point position (N or E)
a : secular velocity vector
b : logarithmic constant
c : coseismic offset
t : time after the main shock
tq : time when the main shock occurred
$t\log$: decay time

The logarithmic model has a period of rapid increase, followed by a period where growth slows down, but growth continues to increase independently. This makes the model unsuitable where there needs to be an upper and a lower limit. This study uses upper and lower values to limit the smoothing to make it faster and more rational.

Equation (3), has parameters in the form of a secular velocity vector as a result of postseismic correction logarithmic constant (b), coseismic offset (c), and half-life (t log). These parameters are

determined by the least square method of the parameter method according to equation (2), where the matrix X contains the parameters *a*, *b*, *c,* and *t* log.

After the velocity values of the components E, N, and U are obtained, then the resultant value of horizontal velocity (*Vhz*) is searched by equation (4) of the velocity parameter values E (*Ve*) and velocity N (*Vn*).

$$Vhz = \sqrt{(Ve)^2 + (Vn)^2} \tag{4}$$

In this case,

Vhz : resultant of point displacement velocity vector
Ve : point displacement velocity in E component
Vn : point displacement velocity in N component

After the velocity value and its standard deviation in the topocentric coordinate system are obtained, then the visualization is carried out with GMT.

The comparison of the velocity results from the calculation with the linear least square and the logarithmic methods was carried out using the two-parameter difference significance test. The test requires velocity vector data for each observation station on the results of the two methods as well as the standard deviation. This test is done by calculating the t-value with equation (5) which is then compared to the t-value in the Student distribution (t-table).

$$t = \left(\frac{x_{1-}\, x_2}{\sigma^2\, x_1 + \sigma^2\, x_2}\right) \tag{5}$$

In this statistical test, the degree of freedom (df) value is infinite (∞) with a confidence level of 95% (α = 5%) so that the t-table value is 1.96. If the t-value > t-table ($t_{df,\alpha/2}$), it shows the rejection of Ho which concludes that the velocity has a significant difference.

3. Results and Discussion

3.1. Evaluation Result of Time Series Coordinates of the Opak Fault Monitoring Station GAMIT/GLRED Processing Results

In this study, GAMIT was used to obtain daily solutions from GNSS observational data. The results of GAMIT processing are in the form h-file and sh_gamit_summary. The checking the quality of GAMIT processing data can be seen from the fract and postfit nrms values that are in the h-file every doy. If the fract and postfit nrms values match the criteria, it indicates that the data is free from blunder and systematic errors.

The processing with the GLRED module obtained time series values in the form of coordinates and standard deviation of each station. The resulting coordinates and standard deviation are in the form of a 3D cartesian coordinate system (X, Y, and Z) and a topocentric coordinate system, namely E, N, and U.

This study uses topocentric coordinates for analysis. The topocentric coordinate system is a local coordinate system in the form of E, N, and U tied to the direction of the normal line of the reference ellipsoid at a point on the earth's surface. The data format containing the date of observation, E, N, and U coordinate data is used for plotting time series data also calculating the fitting and velocity values. Figure 3.1 is a part of the results of the CORS JOG2 data conversion.

JOG2.ER - Notepad

File Edit Format View Help

```
2011-05-03 0.03008 0.00371 -0.10290 0.00534 0.04204 0.01552
2011-05-04 0.02788 0.00527 -0.09741 0.00750 0.03383 0.03066
2011-05-05 0.03332 0.00331 -0.10360 0.00481 0.00780 0.01334
2011-05-06 0.03579 0.00413 -0.10677 0.00600 -0.00096 0.01913
2011-05-07 0.03105 0.00390 -0.10004 0.00559 -0.01774 0.01841
2011-05-08 0.03276 0.00369 -0.10493 0.00521 -0.00028 0.01782
2011-05-09 0.03502 0.00374 -0.10313 0.00505 0.00661 0.01573
2011-05-12 0.03088 0.00747 -0.11071 0.00982 0.07134 0.12054
2011-05-13 0.03134 0.00526 -0.09919 0.00662 0.01018 0.03770
2011-05-15 0.03258 0.00575 -0.09682 0.00784 0.00017 0.04510
2011-05-16 0.02936 0.00469 -0.10627 0.00612 0.00294 0.03024
2011-05-29 0.03365 0.00527 -0.10245 0.00664 0.04408 0.04112
2011-10-29 0.02903 0.00692 -0.08795 0.01023 0.00272 0.04533
2011-12-03 0.02731 0.00532 -0.09047 0.00730 0.03057 0.02197
2011-12-04 0.02849 0.00474 -0.09436 0.00681 0.02896 0.02285
2011-12-05 0.02328 0.00597 -0.09193 0.00857 0.01821 0.02961
2011-12-06 0.02600 0.00535 -0.09330 0.00723 0.00994 0.02515
2011-12-07 0.02764 0.00500 -0.09384 0.00719 0.00661 0.02370
2011-12-08 0.02597 0.00508 -0.09222 0.00719 0.00959 0.02044
2011-12-09 0.02736 0.00509 -0.09227 0.00771 0.02846 0.02090
2011-12-11 0.02895 0.00553 -0.09176 0.00802 -0.00926 0.02252
2011-12-12 0.02099 0.00458 -0.09257 0.00656 -0.01195 0.01784
2011-12-13 0.02458 0.00456 -0.08656 0.00651 0.01235 0.02055
2011-12-14 0.02441 0.00489 -0.09154 0.00725 -0.00621 0.02201
```

Figure 3.1. Part of the converted JOG2.ER file.

Figure 3.1 contains the date of observation, the value of the displacement of the E, N, and U coordinate stations along with the standard deviation of Se, Sn, and Su.

3.1.1. Plotting Time Series and Fitting

The results of plotting time series and fittings for the CORS JOG2 station and monitoring stations TGD1 and SGY6 are presented in Figures 3.2 to 3.4. CORS JOG2 station is continuous CORS Yogyakarta data. TGD1 and SGY6 are part of several Opak Fault observation station.

Figure 3.2 to 3.4 shows a part of the time series displacement and logarithmic fittings of the CORS JOG2, TGD1, and SGY6 stations. The time series of GNSS data is used in this research. The blue dot shows the plotting of time series data for GNSS observations, the black line shows the suitability of the linear least square function, and the red line shows the best fit of the logarithmic function.

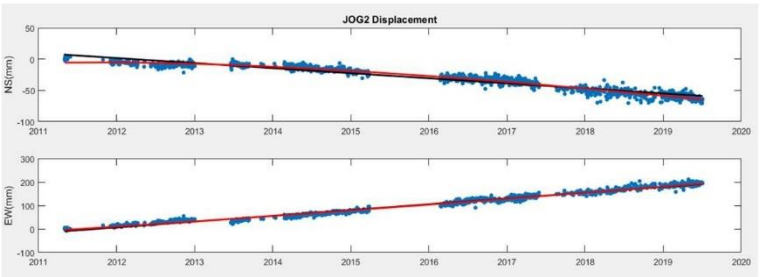

Figure 3.2. Part of *time series displacement* and logarithmic *fitting* of the CORS JOG2 observation station. (Abdiana, 2020)

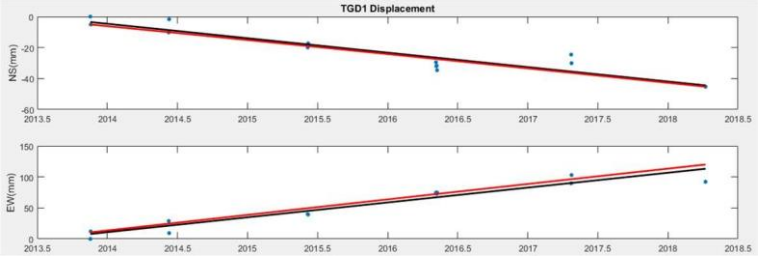

Figure 3.3. Part of time series displacement and logarithmic fitting of TGD1 observation station.

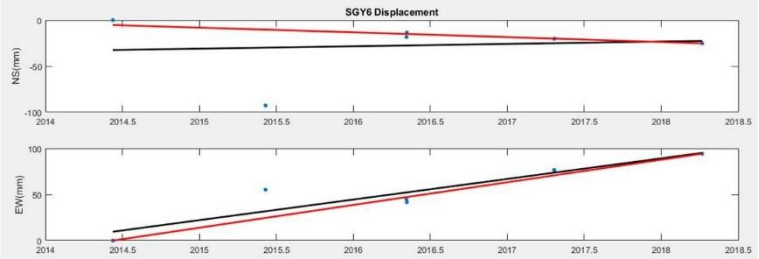

Figure 3.4. Part of time series displacement and logarithmic fitting of SGY6 observation station.

Figure information 3.2 to 3.4:
Blue : time series data of GNSS observation
Black : linear least square function
Red : logarithmic function

Based on the results of this time series plotting, it can be seen that the changes in the position of the E and N components in millimeter fractions. In Figures 3.2 and 3.3, it can be seen that the plotting and fitting shows the stations have the same line pattern. In the N component the line goes down indicating the movement to the south and in the E component the line moves up which indicates the movement to the east, so that the station movement moves to the southeast. The plotting linear least square and logarithmic methods also seen coincided, indicating that the two methods have almost the same value.

However, the SGY6 station in Figure 3.3, has a slight difference. The E component as a result of plotting and the fit line moves up, indicating its movement to the south, while the E component tends to move straight, so that the SGY6 station movement is heading east. The plotting linear least square and logarithmic also shows a significant difference compared to other stations. This can be seen because there are station points in 2015 that are slightly different from other station points which are in the linear least square and logarithmic line. This can indicate that SGY6 station has poor accuracy and suitability which causes the RMS error value to be greater than the other stations. Based on Figure 3.2 to 3.4 also shows that there were several jumps between the years of observation, especially the range from 2013 to 2018. This can be indicated because of the influence of earthquake activity during that period in the Yogyakarta area.

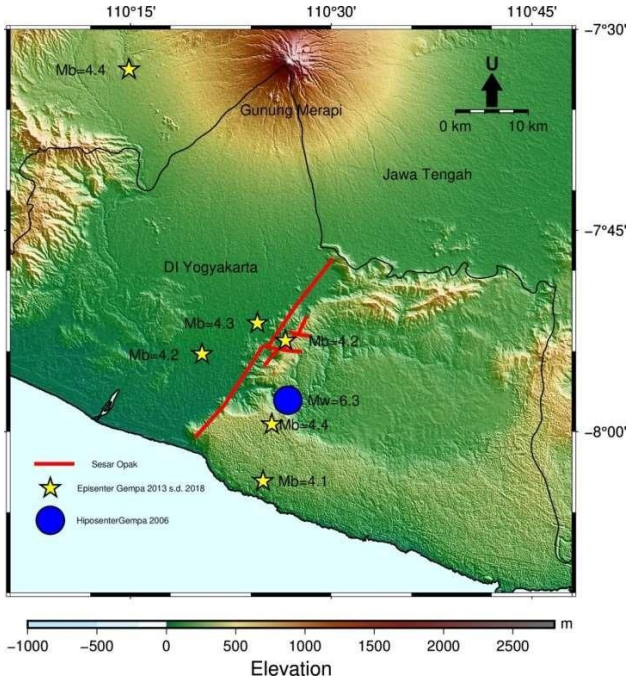

Figure 3.5. Distribution of earthquakes that occurred in the Opak Fault area from 2013 to 2018. Hypocenter location taken from https://earthquake.usgs.gov.

Figure 3.5 shows the distribution of earthquakes with a magnitude of more than 4 Mb that occurred in the Opak Fault area during the period 2013 to 2018 along with the hypocenter of the 2006 earthquake that occurred with a magnitude of 6.3 Mw in Yogyakarta based on USGS data. The image illustrates the tectonic activity in the Opak Fault area which affects the time series value of the observation station. The earthquake from 2013 to 2018 occurred in Yogyakarta with magnitudes ranging from 4.1 Mb to 4.4 Mb based on USGS data retrieved through https://earthquake.usgs.gov.

Based on Figures 3.2 and 3.3, the results of time series plotting on components E and N increased between 2013 to 2014. This was due to the postseismic effect of an earthquake with a magnitude of 4.1 Mb on April 2, 2013 in 16 km southwest Moyudan and November 14, 2013 in 14 km southeast of Pundong which affects the observation solution. Based on Figure 3.2 to 3.4, in 2014 to 2015, there was a slight decrease in the N component. This occurred due to the effect of the earthquake on April 2, 2014 with a magnitude of 4.2 Mb in 9 km east of Sewon, and an earthquake of 4.3 Mb on May 13, 2015 at 5 km northeast of Sewon as well as the earthquake on September 25, 2015 with a magnitude of 4.4 Mb in 9 km southeast of Pundong. The postseismic influence of the three earthquakes still affects the observation solution. Meanwhile, in 2015 to 2016, there was an increase in components E and N. In this phase, it is estimated that energy accumulation occurs because in this phase there is no earthquake. In 2016 to 2017, the increase was insignificant. This is due to the effect of the earthquake that occurred on July 17, 2016 with a magnitude of 4.4 Mb in 4 km southeast of Mertoyudan and the earthquake on January 13, 2017 with a magnitude of 4.2 Mb in 2 km southeast of Bantul, did not have a significant effect because it was far from the fault location. Meanwhile, between 2017 and 2018 there was an earthquake on 20 July 2017 at 113 km south of Pundong, Bantul with a magnitude of 4.7 Mb, and 11 August 2017 with a magnitude of 4.3 Mb in 54 km southwest of Bambanglipuro, and January 22, 2018 with a magnitude of 4.4 Mb in 115 km southwest of Bambanglipuro which is estimated to affect the monitoring station insignificantly. Therefore, the E and N components decreased which was not significant. This can be caused by the distance of the earthquake which is quite far from the observation station. Apart from the effects of the postseismic earthquake in 2013 to 2018, the postseismic impact of the Yogyakarta earthquake on May 27, 2006 is also estimated to have affected. This is in accordance

with research (Abidin, et al., 2009) which explains that the postseismic effects of the 2006 Yogyakarta earthquake continued for several years afterwards.

3.1.2. The RMS error value for each station.

In its processing, evaluation goodness of fit uses the RMS error to determine the fit of the model. The RMS error results are shown in Table 3.1. and 3.2. The RMS error value is used to determine how much error occurs in the calculation of the model and to evaluate the suitability of the model used. The smaller the RMS error value, the smaller the error that occurs in using the model. The RMS error value with a RMSE value <1 m or a value close to 0, the accuracy is getting better. This shows that the model has a smaller random error component and has a better suitability for predictions.

The average RMS error value of the monitoring station linear least square method is 18.041 mm, with values ranging from 7.321 to d. 45.518 mm. The resulting RMS error value is quite good, with a value of less than 1 cm. However, when viewed from all stations, SGY6 station has the greatest value compared to other stations with a total RMS error value of 45.518 mm. The results of the RMS error value for all stations are presented using the graph in Figure 3.6.

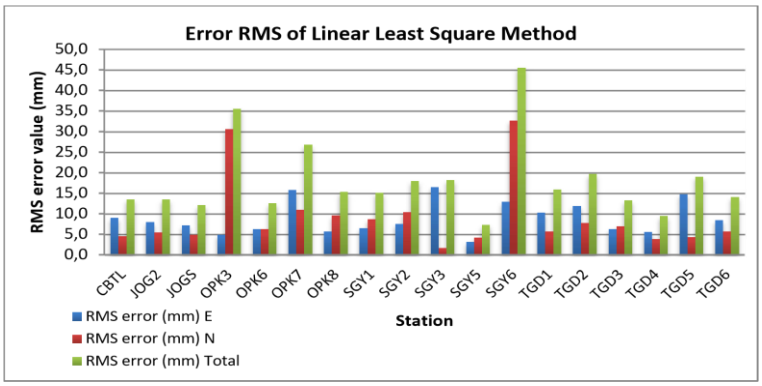

Figure 3.6. RMS error of the linear least square method.

Figure 3.6 presents a graph of the RMS error using the linear least square method. It can be seen on the graph that the RMS error value obtained varies considerably with a value below 45 mm, this means that the value is still below 1 cm. SGY6 station's RMS error value which is greater than other stations indicates that SGY6 station has a larger random error component, and has less accuracy and suitability for prediction than other stations.

The average RMS error value for the logarithmic method of the monitoring station has an RMS error value of 16.970 mm, with values ranging from 7.700 to 34.127 mm. The results of the RMS error value for all stations using the logarithmic method are presented in Figure 3.7.

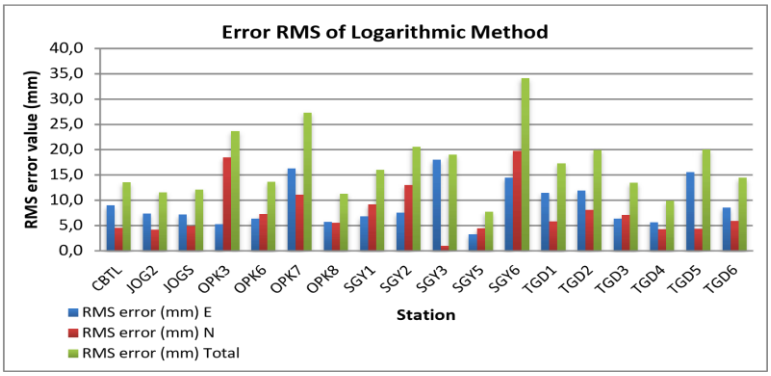

Figure 3.7. RMS error of the logarithmic method.

Figure 3.7 presents an RMS error graph using the logarithmic method. It can be seen on the graph that the RMS error value obtained varies considerably with a value below 35 mm, this means that the value is still below 1 m. The largest value is at the SGY6 station with a total RMS error value of 34.127 mm. This indicates that SGY6 station has a bigger random error component, and has less accuracy and suitability for prediction than other stations.

Figures 3.6 and 3.7 show that the SGY6 station has a large RMS error value, with a total of 45.518 mm in the linear least square method and 34.127 mm in the logarithmic method. This is because the data for the station is not good, it can be seen in the plotting time series of SGY6 station in Figure 3.4, there is data in 2015 that deviates slightly from the suitability of the linear least square and the logarithmic function lines. Therefore, it is indicated to be the cause of the large error RMS value. The average RMS error value for each station used the linear least square and the logarithmic methods, namely 18.041 mm and 16.970 mm. This shows that the difference in the RMS error value is not too different, only different from 1.071 mm. But the logarithmic method has a smaller value than the linear least square method. This indicates that the fitting with the logarithmic method has better accuracy than the linear least square method when viewed from the resulting RMS error value.

3.2. Vector Velocity of Linear Least Square Movement of the Opak Fault Monitoring Station

The velocity value of the GNSS monitoring station for the Opak Fault is calculated using the linear least square method. The secular velocity of this displacement is obtained in the topocentric coordinate system (N, E, and U). The quality of a good velocity value can be seen from the small standard deviation value. The velocity value is calculated by equation (1). The results of velocity values along with standard deviation are presented in Table 3.1.

Table 3.1 shows the velocity values of the components E, N, and U, and the resultant horizontal displacement velocity of the Opak Fault campaign observation station and the continuous CORS JOG2 results. In component E, all monitoring stations have a positive value which indicates an eastward movement with a velocity of 21.676 to 30.997 mm/year, while in the N component, almost all monitoring stations are negative which indicates a movement to the south with a velocity value of –14.116 to -6.914 mm/year. However, the SGY6 station has a different value, namely 2.573 mm/year, which indicates the point is moving northward. This is similar to the results of the N component velocity vector with reference to the Sunda Block at SGY6 station (Pinasti, 2019) which is also positive, namely 1.264 mm/year. The standard deviation value reaches the millimeter fraction with values ranging from 0.031 to 11.212 mm.

Table 3.1. The secular velocity of the Opak Fault monitoring station.

Station	E (°)	N (°)	*Ve* (mm/yr)	*σe* (mm)	*Vn* (mm/yr)	*σn* (mm)	*Vhz* (mm/yr)	*Vup* (mm/yr)	*σup* (mm)
CBTL	110.34	-7.89	27.20	0,06	-8.42	0.03	28.47	-0.89	0.09
JOG2	110.37	-7.76	24.64	0.10	-8.08	0.06	25.93	-0.70	0.17
JOGS	110.29	-7.82	26.98	0.04	-8.64	0.03	28.33	0.40	0.07
OPK3	110.55	-7.89	30.17	1.60	-9.96	10.05	31.77	15.77	11.76
OPK6	110.55	-7.96	28.59	1.67	-11.09	1.66	30.67	17.24	9.91
OPK7	110.46	-8.04	24.87	4.21	-14.12	2.92	28.60	-0.83	3.26
OPK8	110.40	-7.96	25.59	1.52	-7.98	2.56	26.80	7.02	42.95
SGY1	110.42	-7.88	29.44	1.72	-9.18	2.30	30.84	-11.27	39.31
SGY2	110.40	-7.90	31.00	1.99	-8.70	2.78	32.20	30.89	22.56
SGY3	110.42	-7.90	21.68	5.42	-9.81	0.55	23.79	36.88	7.85

SGY5	110.45	-7.86	24.21	1.03	-9.08	1.38	25.86	15.32	6.51
SGY6	110.47	-7.86	22.36	4.43	2.57	11.21	22.51	3.47	9.59
TGD1	110.49	-7.77	23.98	2.17	-9.32	1.20	25.73	203.91	117.54
TGD2	110.45	-7.88	28.96	2.14	-8.88	1.39	30.29	33.96	6.46
TGD3	110.37	-7.75	27.75	1.26	-10.87	1.41	29.81	-15.45	12.22
TGD4	110.31	-7.85	25.29	1.31	-9.28	0.92	26.94	-15.80	9.43
TGD5	110.20	-7.74	26.15	3.70	-6.91	1.07	27.05	19.64	5.99
TGD6	110.20	-7.91	30.92	1.51	-10.68	1.02	32.71	9.76	2.91

Based on the velocity values in the E and N components, the resultant value of the horizontal velocity for each station is calculated by equation (4). The resultant value of the horizontal velocity for each station ranges from 22.507 to 32.711 mm/year. The vertical velocity value is obtained from the U component velocity value which ranges from -0.89 to 203.91 mm/year with a standard deviation of 0.07 to 117.54 mm.

Figure 3.8 shows the results of the horizontal velocity vector plotting along with its standard deviation and vertical velocity of the Opak Fault monitoring station with GMT. The red line shows the location of the Opak Fault based on Walter's research on (Pinasti, 2019). The blue arrow shows the horizontal velocity vector of the station and its accuracy is denoted by the error ellipse. The error ellipse has a center at the end of the arrowhead. The value of the error ellipse is calculated from the value of the variance of the E and N components. The value of the variance of the component is calculated from the standard deviation value of the E and N components (Yudistira, 2016). The larger the error ellipse, the greater the accuracy value. The vertical velocity obtained from the velocity component U (*Vup*) is represented by a magenta line with the tip of the arrow indicating its direction.

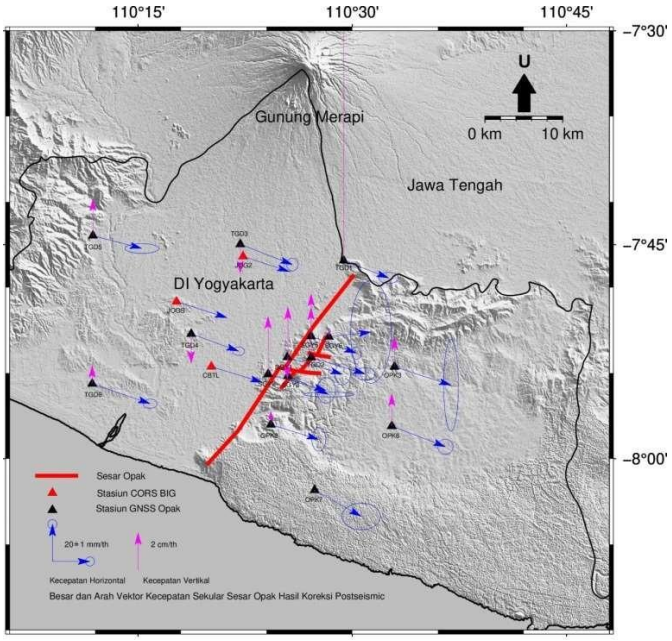

Figure 3.8. Plotting of the secular velocity of the Opak Fault monitoring station. (Abdiana, 2020)

Based on Figure 3.8, the plotting show that all stations have a horizontal component velocity vector that tends to the southeast with relatively the same magnitude. This is in accordance with research (Pinasti, 2019) which is influenced by the subduction process of the Indo-Australian and Eurasian Plates

which results in the Java Trench subduction zone and research (Bock, et al., 2003) that in the Southern Southern Mountains Region it tends to follow the direction of movement due to the influence subduction zone. The movement of the Java Island station tends to move to the southeast due to the movement of tectonic plates. However, the SGY6 station has a different direction, points to the northeast. This is similar to the results of the horizontal velocity vector visualization with the reference to the SGY6 Sunda Block station (Pinasti, 2019) which also points to the northeast. As for the vertical velocity it looks not homogeneous, has varying patterns and values. Some components are moving downwards and upwards. This is in accordance with the results obtained based on Table 3.1 which shows the value of the velocity of the U component which varies with a large standard deviation value.

3.3. Vector Velocity of Linear Least Square Movement of the Opak Fault Monitoring Station

The secular velocity of this displacement is obtained in the topocentric coordinate system (N, E, and U). The velocity values along with the standard deviation using the logarithmic method are obtained as in Table 3.2.

Table 3.2 shows the velocity values of the E, N, and U components, and the resultant horizontal displacement velocity of the Opak Fault campaign observation station and the CORS BIG continuous observation. In component E, all monitoring stations have a positive value which indicates an eastward movement with a velocity of 20.735 to 29.864 mm/year, while in the N component all monitoring stations are negative which indicates a movement to the south with a velocity value of -22.255 to -6.439 mm/year. The standard deviation value reaches the millimeter fraction with a value ranging from 0.318 to 6.767 mm.

Based on the velocity values on the E and N components, the resultant value of the horizontal velocity for each station is calculated with equation (4). The resultant value of the horizontal velocity for each station ranges from 36.963 to 23.281 mm/year. The vertical velocity value is obtained from the U component velocity value which ranges from -30 to NaN mm/year with a standard saving value of 3.00 to NaN. Figure 3.9 shows the results of plotting the secular velocity of the postseismic correction of the Opak Fault monitoring station with GMT.

Figure 3.9 shows the horizontal and vertical velocity vectors plotting along with the standard deviation. The red line shows the location of the Opak Fault based on Walter's research on (Pinasti, 2019). The blue arrow shows the horizontal velocity vector of the station and its accuracy is denoted by the error ellipse. The error ellipse has a center at the end of the arrowhead. The error ellipse value is calculated from the variance value of E and N components. The variance value of the component is calculated from the standard deviation value of E and N components (Yudistira, 2016). The larger the error ellipse, the greater the accuracy value. The vertical velocity obtained from the velocity component U (Vu) is represented by a magenta line with the tip of the arrow indicating its direction.

Table 3.2. The secular velocity vector with postseismic correction.

Stations	E (°)	N (°)	*Ve* (mm/yr)	*σe* (mm)	*Vn* (mm/yr)	*σn* (mm)	*Vhz* (mm/yr)	*Vup* (mm/yr)	*σup* (mm)
CBTL	110.34	-7.89	29.52	2.64	-8.72	1.30	30.78	-6.26	3.45
JOG2	110.37	-7.76	29.51	4.43	-22.25	3.12	36.96	21.30	7.88
JOGS	110.29	-7.82	27.31	0.51	-8.52	0.32	28.61	8.46	11.75
OPK3	110.55	-7.89	29.37	1.72	-8.41	6.05	30.55	25.37	7.08
OPK6	110.55	-7.96	27.56	1.70	-10.25	1.93	29.41	9.31	10.64
OPK7	110.46	-8.04	24.18	4.33	-14.63	2.95	28.27	1.90	3.76
OPK8	110.40	-7.96	24.69	1.52	-9.84	1.49	26.58	-30.00	48.15
SGY1	110.42	-7.88	28.78	1.81	-9.57	2.45	30.33	NaN	NaN
SGY2	110.40	-7.90	29.08	2.01	-12.26	3.46	31.56	1.28	13.02
SGY3	110.42	-7.90	20.73	5.91	-10.59	0.33	23.28	23.09	4.99

SGY5	110.45	-7.86	23.69	1.08	-10.09	1.45	25.75	11.55	6.92
SGY6	110.47	-7.86	23.38	4.96	-6.44	6.77	24.25	-5.62	5.78
TGD1	110.49	-7.77	23.67	2.43	-10.44	1.23	25.87	NaN	NaN
TGD2	110.45	-7.88	27.15	2.14	-10.77	1.44	29.21	26.09	6.72
TGD3	110.37	-7.75	26.42	1.28	-12.66	1.43	29.29	3.26	5.75
TGD4	110.31	-7.85	24.39	1.33	-9.38	1.00	26.13	-9.90	10.10
TGD5	110.20	-7.74	26.78	3.90	-8.34	1.10	28.04	15.30	6.09
TGD6	110.20	-7.91	29.86	1.53	-11.55	1.05	32.02	10.93	3.00

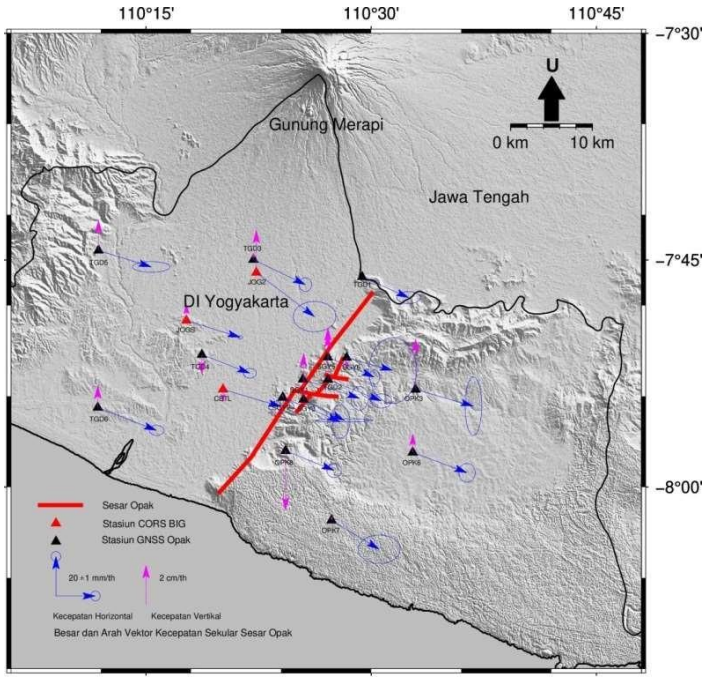

Figure 3.9. Plotting of secular velocity of with postseismic correction of the Opak Fault monitoring station.

Based on Figure 3.9, the plotting show that all stations have a horizontal component velocity vector that tends to the southeast with relatively the same magnitude. The results of the secular velocity value visualization are almost similar to the linear least square method (Figure 3.8). As for the vertical velocity it looks not homogeneous, some of the components are moving downwards and upwards. This is the same as the value of secular velocity without correction where the vertical velocity varies and cannot describe the secular motion. The errors in the U component can be caused by the GNSS vertical accuracy which is less good than the horizontal accuracy as well as the error in the height measurement of the tool. This is due to the satellite geometry that does not allow observations below the horizon so that the net bond strength for the vertical or high component is weaker. In addition, the existence of several biases such as tropospheric bias also affects the level of accuracy, namely reducing the more accuracy of the vertical component. In addition, the vertical component error is also greatly influenced by the inaccurate height of the antenna (Fadhilah, 2019). The deformation modeling in this next study can be tried without vertical components because it has a significant effect, so that this vertical velocity value is no longer used in the process of secular velocity comparison analysis.

3.4. Comparison of Secular Velocity without Correction and Secular Velocity of Postseismic Correction Results

Based on the velocity results in Tables 3.1 and 3.2, a comparison of the secular velocity without correction was carried out with the secular velocity of the postseismic correction. Table 3.3 is the result of calculating the difference between the secular velocity vectors using the linear least square method and the secular velocity with the postseismic correction results using the logarithmic method.

Table 3.3. The difference in secular velocity values.

Stations	Δ*Ve* (mm/year)	Δ*Vn* (mm/year)	Δ*Vhz* (mm/year)
CBTL	-2.323	0.295	-2.309
JOG2	-4.876	14.175	-11.035
JOGS	-0.329	-0.118	-0.278
OPK3	0.806	-1.543	1.225
OPK6	1.027	-0.843	1.260
OPK7	0.688	0.518	0.331
OPK8	0.901	1.866	0.226
SGY1	0.663	0.398	0.509
SGY2	1.915	3.561	0.634
SGY3	0.941	0.773	0.513
SGY1	0.663	0.398	0.509
SGY2	1.915	3.561	0.634
SGY3	0.941	0.773	0.513
TGD2	1.808	1.890	1.081
TGD3	1.336	1.788	0.513
TGD4	0.904	0.099	0.811
TGD5	-0.624	1.424	-0.994
TGD6	1.054	0.872	0.691

Table 3.3 shows the difference in velocity values for the E and N components along with the difference in horizontal velocity. The difference in velocity values in component E ranges from -4.876 to 1.915 mm/year, and the N component ranges from -1.543 to 14.175 mm/year. The difference in the horizontal velocity values ranges from -11.035 to 1.260 mm/ year. The biggest difference in velocity values is JOG2 and SGY6 stations. The difference of secular velocity values of JOG2 station for the Δ*Ve*, Δ*Vn*, and Δ*Vhz* components has a greater value than the other stations. The difference of secular velocity values of SGY6 station for the Δ*Vn* component has a large value. Then, the comparison of the secular velocity values of the two methods is visualized with GMT.

Figure 3.10 can be seen visually that the velocity value between the two methods has changed, but there is no significant change in velocity between the secular velocity (black arrow) and the secular velocity as a result of the postseismic correction (blue arrow). The difference is significant, namely JOG2 and SGY6 stations. Overall, the station is directed southeast.

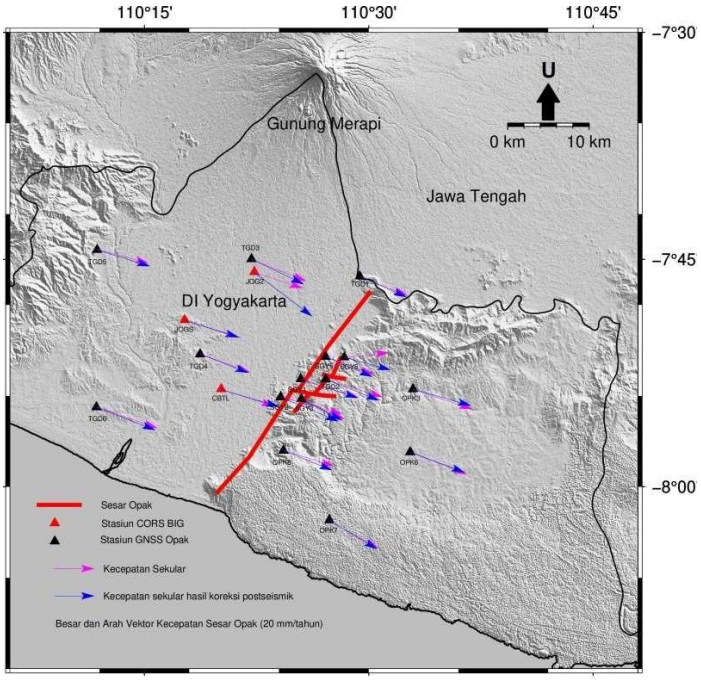

Figure 3.10. The comparison of the secular velocity without and with postseismic corrections.

The velocity obtained from the linear least square and the logarithmic methods does not much different. Then, postseismic does not have a significant impact on secular velocity, the calculation of secular velocity is sufficient to use the linear least square method without postseismic correction with the logarithmic method.

3.5. Significance Test for Difference of Two Secular Velocity Parameters

In this study, the two-parameter difference significance test was carried out on the secular velocity of processing results using the linear least square and the logarithmic methods. The test was conducted to determine whether the displacement velocity of the two processes was significantly different or not. This test is done by calculating the t-value with equation (5), then comparing it with the t-value in the Student distribution (t-table). This statistical test used the 95% confidence level and df = ∞, the t-table value is 1.96.

Figure 3.11 shows the graph of the results of the t-value test of the difference between the two components *Ve* and *Vn* for all stations. On the results of the *Ve* component test, the t-value ranges from 0.10 to. 1.10 so that the hypothesis is accepted. It indicates that the secular velocity value *Ve* is not significantly different. The results of the *Vn* component test, the t-value ranges from 0.12 to. 1.20 for seventeen stations so that the hypothesis is accepted, thus indicating that the value of the secular velocity *Vn* is not significantly different. However, the JOG2 station has a value of t-value up to 4.54 so that it concludes that the value is significantly different.

It can be seen in the graph in Figure 3.11 that the t-value above 1.96 is found in the *Vn* component of the JOG2 station. The t-value for other observation stations, the t-value is below 1.96 which indicates that the secular velocity of the station is not significantly different.

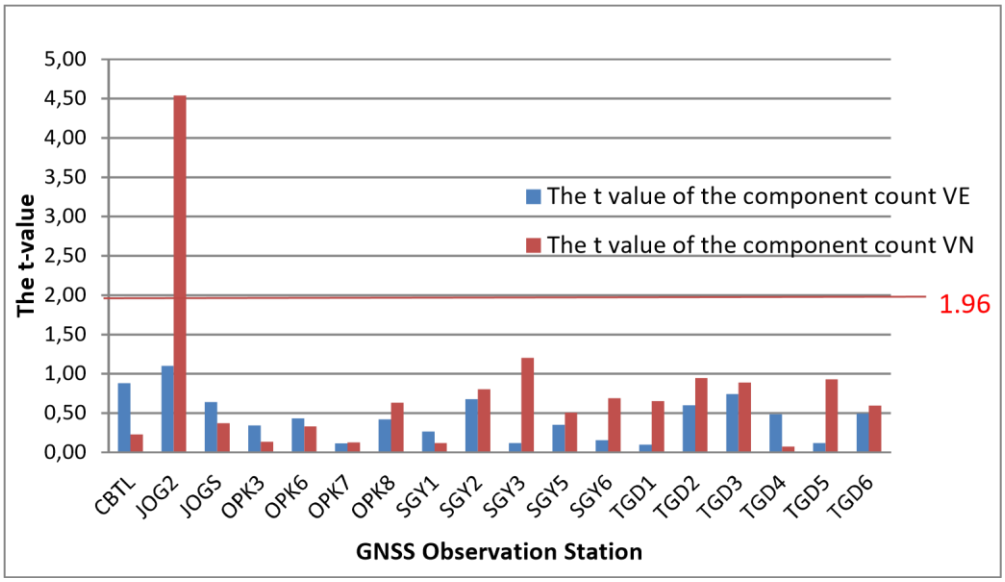

Figure 3.11. Graph of the difference in secular velocity values.

Based on the two-parameter difference significance test, the results show that the secular velocity of the postseismic correction with and without the correction is not significantly different even though the two value has different results in sub millimeter (Table 3.3). The hypothesis of this study is that postseismic correction has a significant effect on the estimation of secular velocity with an indication that a significant difference between the secular velocity before and after correction has not been fulfilled. This is because of the values obtained by the logarithmic method are not much different from linear least square method.

4. Conclusion

The results of this study show that there is no significant difference in velocity between the secular velocity values without correction using the linear least square method and the secular velocities with the postseismic correction using the logarithmic method. The secular velocity is sufficient using the linear least square model without postseismic correction with the logarithmic method. The postseismic does not have a significant impact on its secular value.

5. Acknowledgement

The authors thank the anonymous reviewer and editor for valuable comments. We would like to express our deep gratitude to the Geometrical and Physical Geodesy Laboratory for maintaining the GNSS observation. This study was partially supported by Universitas Gadjah Mada in the scheme of Final Project Recognition. Map figures were generated by the Generic Mapping Tools (Wessel, et al., 2013).

6. Conflict of Interest Statement

The author states there is no conflict of interest in this article.

References

[1] Abdiana, S.P. (2020). Kecepatan Sekular Stasiun Pengamatan GNSS Sesar Opak Pascagempa 2006 Yogyakarta. Universitas Gadjah Mada.

[2] Abidin, H.Z., Andreas, H., Meilano, I., Gamal, M., Gumilar, I., and Abdullah, C.I. (2009). Deformasi Koseismik dan Pascaseismik Gempa Yogyakarta 2006 dari Hasil Survei GPS, (January 2016). https://doi.org/10.17014/ijog.v4i4.87.

[3] Bock, Y., Diego, S., and Mccaffrey, R. (2003). Crustal Motion in Indonesia from Global Positioning System Measurements, (August). https://doi.org/10.1029/2001JB000324.

[4] Fadhilah, F. (2019). Pergeseran Stasiun Pemantauan Sesar Opak dengan Pengolahan Data GNSS Multitahun (2013 s.d. 2018) Mengacu pada ITRF2008 dan ITRF2014.
[5] Feng, L., Hill, E.M., Banerjee, P., Hermawan, I., Tsang, L.L.H., Natawidjaja, D.H., Sieh, K. (2015). A Unified GPS-based Earthquake Catalog for the Sumatran Plate Boundary between 2002 and 2013, pp. 3566-3598. https://doi.org/10.1002/2014JB011661.
[6] Heliani, L.S., Pratama, C., Parseno, Widjajanti, N., Lestari, D., and Ulinnuha, H. (2019). GPS-Derived Secular Velocity Field around Sangihe Island and its Implication to the Molucca Sea Seismicity, Geomatika, vol. 26, no 2. http://dx.doi.org/10.24895/JIG.2020.26-2.1199.
[7] Maiyudi, R., Meilano, I., and Sarsito, D. (2017). Akumulasi Regangan di Sumatera Berdasarkan Data Pengamatan GPS Tahun 2002-2008 dan Dampak Kerusakan Lingkungan Akibat Pelepasan Regangan. Jurnal Rekayasa Hijau, I(2), pp. 89-99.
[8] Marone, C.J., Scholtz, C.H., and Bilham, R. (1991). On the Mechanics of Earthquake Afterslip, (May). https://doi.org/10.1029/91JB00275.
[9] Pinasti, A. (2019). Pemodelan Deformasi Kawasan Sesar Opak Berdasarkan Data GNSS Periodik Tahun 2013 sampai 2018. Universitas Gadjah Mada.
[10] Pusat Gempa Nasional. (2017). Peta Sumber dan Bahaya Gempa Indonesia Tahun 2017.
[11] Stanaway, R., Roberts, C., Blick, G., Crook, C., and Zealand, N. (2012). Four Dimensional Deformation Modelling , the Link between International, Regional, and Local Reference Frames Four Dimensional Deformation Modelling , the Link between International , Regional and Local Reference Frames, (May 2012),pp. 6-10.
[12] Wessel, P., Smith, W.H.F., Scharroo, R., Luis, J., Wobbe, F. (2013). Generic Mapping Tools: improved version released. EOS Trans AGU, 94(45), pp. 409-410. https://doi.org/10.1002/2013EO450001
[13] Widjajanti, N., Pratama, C., Parseno, Sunantyo, T.A., Heliani, L.S., Ma'ruf, B., Atunggal, D., Lestari, D., Ulinnuha, H., Pinasti, A., and Ummi, R.F. (2020). Present-day Crustal Deformation revealed Active Tectonics in Yogyakarta, Indonesia Inferred from GPS Observations. *Geod. Geodyn.*, vol. 11, no. 2, pp. 135-142. https://doi.org/10.1016/j.geog.2020.02.001.
[14] Widjajanti, N., Emalia, S.S., and Parseno. (2018). GNSS Monitoring Network Optimiation Case Study: Opak Fault Deformation. https://doi.org/10.22146/jgise.38458.
[15] Yudistira, M.F. (2016). Analisis Gerakan 3D Stasiun CORS dan Regangan Akibat Gempa Tektonik Berkekuatan 4 s.d. 5 SR pada Kawasan Pegunungan Selatan Bagian Barat Pulau Jawa. Universitas Gadjah Mada.